# Optimal Imaging of Remote Bodies Using Quantum Detectors

L. A. Howard,[1] G. G. Gillett,[1] M. E. Pearce,[2] R. A. Abrahao,[1] T. J. Weinhold,[1] P. Kok,[2] and A. G. White[1]
[1]*Centre for Engineered Quantum Systems, School of Mathematics and Physics, University of Queensland, 4072 Brisbane, Australia*
[2]*Department of Physics and Astronomy, University of Sheffield, Sheffield S3 7RH, United Kingdom*

(Received 11 April 2019; published 30 September 2019)

We implement a general imaging method by measuring the complex degree of coherence using linear optics and photon number resolving detectors. In the absence of collective or entanglement-assisted measurements, our method is optimal over a large range of practically relevant values of the complex degree of coherence. We measure the size and position of a small distant source of pseudothermal light, and show that our method outperforms the traditional imaging method by an order of magnitude in precision. Finally, we show that a lack of photon-number resolution in the detectors has only a modest detrimental effect on measurement precision and simulate imaging using the new and traditional methods with an array of detectors, showing that the new method improves both image clarity and contrast.

DOI: 10.1103/PhysRevLett.123.143604

Imaging is, at its heart, a multiparameter metrology problem, where physical characteristics of the object are encoded as parameters in the quantum state of light. Quantum metrology studies how to best measure physical quantities in the quantum regime: particularly the measurement precision of parameters that do not have an associated quantum observable—such as phase or time—and estimating the optimal quantum measurement observable from which the parameter can be estimated [1]. Of special interest is the estimation of multiple parameters where the optimal measurement observables for two or more parameters may not be simultaneously comeasurable—e.g., when the observables do not commute. Quantum metrology provides bounds on the achievable precisions of these parameters and determines jointly optimal measurement strategies [2].

It is well known that there are physical limits to the precision with which an image can be formed. The Rayleigh-Abbe-Sparrow limit states that the size of the smallest resolvable features is determined by the ratio of the wavelength and the numerical aperture. There are ways in which this limit can be circumvented, for example using super-resolution techniques that exploit the physical structure of the object [3–5] or object illumination with entangled states of light [6–11]. However, in many applications—for example when the object is very far away—we cannot directly interact with the object, or illuminate it with entangled light: the quantum state of the light field is all that is accessible to the observer. Given a finite size imaging system in the far field—i.e., systems with a finite effective numerical aperture—we here investigate the best way to extract the spatial characteristics of the light source.

Recently, Tsang *et al.* showed that the far field quantum state of light retains a significant amount of information about the separation of two identical incoherent point sources, even when their angular separation approaches zero [12]. Moreover, this information can be extracted with a suitable measurement [13], for example using spatial-mode demultiplexing [14]. Recently, a series of experiments demonstrated sub-Rayleigh resolution for two incoherent point sources, using image inversion interferometry [15,16], digital holography [17], and $\mathrm{TEM}_{01}$ heterodyne detection [18]. However, the retention of the spatial information seems to be restricted to highly symmetric sources [19], and it is an open question how we can optimally extract the spatial characteristics of arbitrary sources. Possible candidates include conventional telescopes, Hanbury Brown–Twiss interferometry [20,21], or estimating higher-order correlations in the far field [22–24].

In this Letter, we consider the important practical case where we do not know the light source distribution, and therefore do not have a simple theoretical model whose parameters we can estimate. This requires that we measure quantities with a special relation to the source distribution, such as the complex degree of coherence (CDC). The van Cittert–Zernike theorem relates the CDC to the source distribution via a two-dimensional Fourier transform [25], which is easy to evaluate. Pearce *et al.* showed that the CDC, $\gamma(\mathbf{r}_1, \mathbf{r}_2) = |\gamma| e^{i\phi}$, between two points $\mathbf{r}_1$ and $\mathbf{r}_2$ in the imaging plane can be measured nearly optimally using the setup in Fig. 1 [26]: the two main features are the application of a varying phase, $\phi_a$, to one mode of incoming light and the measurement using photon-number-resolving detectors. Given the latter, we label this the "Count" scheme. Importantly, since the optimal method involves measurement of noncommuting observables, the Count scheme represents the optimal experimentally achievable scheme, and achieves something very close to the optimal theoretical precision until $|\gamma|$ approaches approximately 0.8.

 

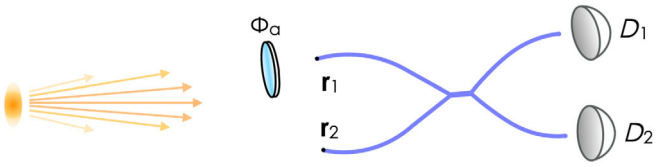


FIG. 1. Schematic for the Count, Traditional, and Click schemes for estimating the complex degree of coherence (CDC) of the light field at positions $\mathbf{r}_1$ and $\mathbf{r}_2$. (This arrangement provides a general imaging procedure since the CDC is directly related to the Fourier transformation of the source distribution via the van Cittert–Zernike theorem). The incoming light fields at $\mathbf{r}_1$ and $\mathbf{r}_2$ are interfered at a beam splitter, the output of which is sent to detectors $D_1$ and $D_2$. In the Count scheme the detectors are photon-number resolving and the phase shift $\phi_a$ is random; the Traditional scheme is similar except the phase is fixed. In the Click scheme the phase is random but the detectors are not number resolving, instead recording events if one or more photons are present.

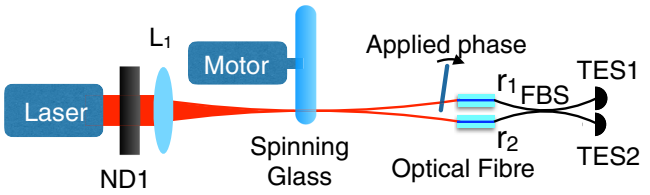


FIG. 2. A 10 kHz pulsed 820 nm laser is attenuated with a neutral density filter (ND1) and focused on a ground glass plate, the rotation of which turns spatially coherent light into spatially incoherent (thermal) light. In the far field, the light is collected into two optical fibers $\mathbf{r}_1$ and $\mathbf{r}_2$ with a glass plate located in front of $\mathbf{r}_1$. As the plate rotates, it applies a relative phase shift $\phi_a$. Both arms are connected to a 50:50 fiber beam splitter (FBS). The outputs are connected to two Transition Edge Sensors, TES1 and TES2, which measure incoming photons in the photon-number basis with single photon-number resolution and near-unit quantum efficiency.

Here, we experimentally implement the Count scheme, comparing it to two alternative schemes both of which are variations of the apparatus in Fig. 1. The first of these is the two-mode analog to a traditional lensing and intensity measurement setup: this "Traditional" scheme replaces the variable phase with a fixed phase. In contrast, the second scheme retains the variable phase but uses detectors that are not photon-number resolving: in this "Click" scheme the detectors merely record an event when one or more photons are present, similar to avalanche photodiode detectors.

Optimality of a scheme is defined via the mean squared error (MSE) in the parameters using unbiased estimators. The quantum Cramér-Rao bound relates the MSE matrix for these parameters to the quantum Fisher information matrix determined by the light field captured in the detectors [26,27]. The quantum Fisher information in turn determines the optimal measurement observables, leading to the setup in Fig. 1. While the parameters of interest $|\gamma|$ and $\phi$ have noncommuting measurement observables, they turn out to be jointly measurable [26].

The coherence, CDC, is determined directly from interference fringes between two spatially separated optical modes in the far field. Light at positions $\mathbf{r}_1$ and $\mathbf{r}_2$ acquires a relative applied phase shift $\phi_a$ (using the phase shifter in Fig. 1), then interferes on a 50:50 beam splitter, and is finally detected by photon-number-resolving detectors $D_1$ and $D_2$, with $x$ being the number of photons in detector $D_1$ and $y$ the number of photons in $D_2$. Post selecting on different photon-number coincidence events $[x, y]$ gives rise to different interference fringes, as illustrated in Fig. 2 in the Supplemental Material [28]. (Note that these calibration fringes are not used for the experimental estimates in Figs. 3 and 4).

The phase $\phi$ of the CDC contains the information about the position of the source relative to the optical axis connecting the source and the imaging plane. To see this, we note that a transversal shift of the source in the direction parallel to $\mathbf{r}_1 - \mathbf{r}_2$ produces a relative phase shift in the optical modes at $\mathbf{r}_1$ and $\mathbf{r}_2$. This results in a translation of the interference fringes. The phase $\phi$ of the CDC is equal to

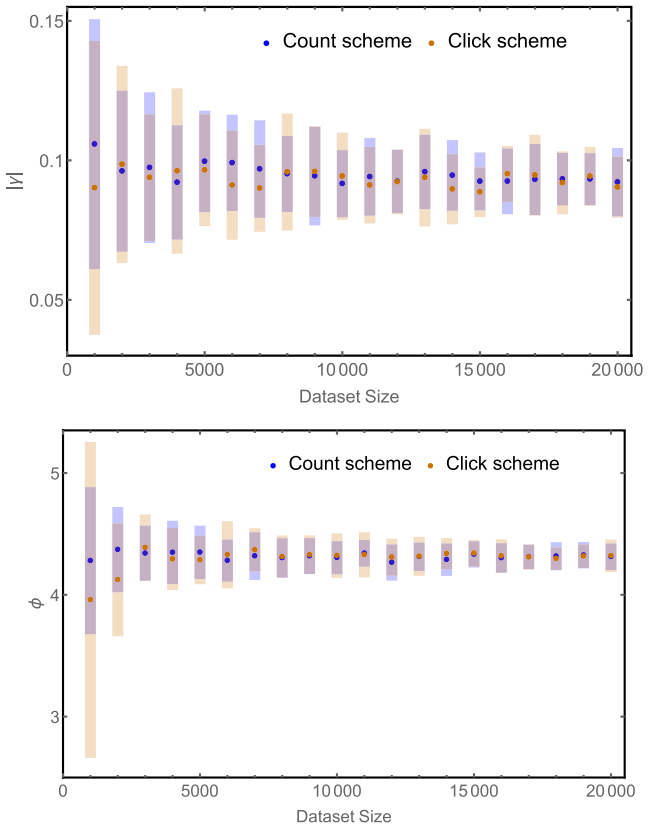


FIG. 3. Count vs Click. Complex degree-of-coherence vs dataset size: Top—magnitude, $|\gamma|$. Bottom—phase, $\phi$. Each point is the mean of 50 trials with the shading representing the standard deviation of the 50 trials. Blue dots and shading are for the Count scheme and orange dots and shading are for the Click scheme. For small data sets, the Count scheme has a clear advantage over the Click scheme; both perform well at large data set sizes.

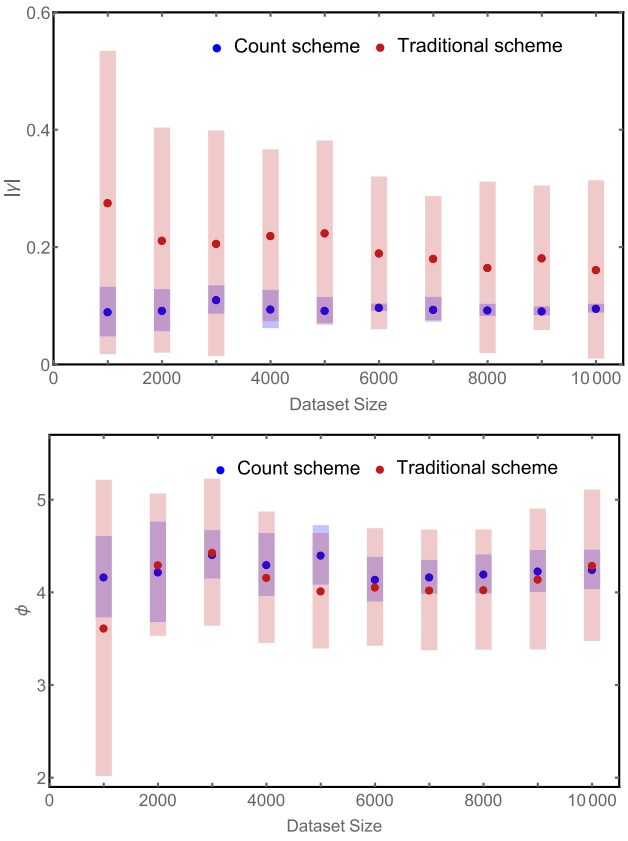


FIG. 4. Count vs Traditional. Complex degree-of-coherence vs dataset size: Top—magnitude, $|\gamma|$. Bottom—phase, $\phi$. Each point is the mean of 20 trials with the shading representing the standard deviation of the 20 trials. Blue dots and shading are for the Count scheme and red dots and shading are for the Traditional scheme. The Count scheme clearly outperforms the Traditional scheme for all dataset sizes.

the applied phase $\phi_a$ at the point where the fringes are all at extremal values. For example, we can infer from Fig. 2 in the Supplemental Material that $\phi$ is slightly less than $\pi$ for the calibration dataset (see the Supplemental Material [28] for more details on the definition and measurement of $\phi$).

The magnitude $|\gamma|$ of the CDC contains the information about the spatial extent of the source, and is equal to the visibility of the fringes,

$$|\gamma| = \frac{I_{\max}^{[x,y]} - I_{\min}^{[x,y]}}{I_{\max}^{[x,y]} + I_{\min}^{[x,y]}}, \tag{1}$$

where $I_{\max}^{[x,y]}$ and $I_{\min}^{[x,y]}$ are, respectively, the maximum and minimum intensity of the interference fringe for detector coincidence events $[x, y]$. To see this, we note that each single point at the source creates an interference fringe with perfect visibility and $|\gamma| = 1$. Incoherent extended sources at different positions then create an incoherent superposition of horizontally translated interference fringes. As the spatial extent of the source increases, the visibility—and hence $|\gamma|$—of the resulting interference fringe decreases. These relationships are formally expressed in the van Cittert–Zernike theorem (see the Supplemental Material [28]).

To extract the values of $|\gamma|$ and $\phi$ from a measured interference fringe we use the maximum likelihood estimator (MLE), which is asymptotically efficient. This means that the variance of the MLE asymptotically approaches the Cramér-Rao bound for large datasets. The MLE optimizes $|\gamma|$ and $\phi$ to fit the experimental data to the probability distribution $\Pr(x, y) = f_{x,y}(\gamma, \bar{n}, \phi_a)$ for detecting a coincidence event $[x, y]$. This distribution is a function of $|\gamma|$, $\phi$, the average photon number $\bar{n}$, and the applied phase $\phi_a$ and is defined explicitly in the Supplemental Material [28].

The experimental apparatus is shown in Fig. 2. Light from a pulsed 820 nm laser diode is spatially filtered using a single-mode fiber, and attenuated to produce a train of weak coherent states with average photon number of approximately one. The single mode is focused to a waist at a ground glass plate that rotates at approximately 5 Hz to create a spatially incoherent light source [29]. The pseudothermal light emanating from the ground glass is collected into two single mode fibers, separated by 48 mm at $\mathbf{r}_1$ and $\mathbf{r}_2$, and located 595 mm from the ground glass plate. In front of the fiber at $\mathbf{r}_1$ we place a rotatable optical flat, the angle of which changes the path length of the light entering the fiber and allows for the application of the variable phase $\phi_a$. The light entering $\mathbf{r}_1$ and $\mathbf{r}_2$ is then interfered on a 50:50 fiber beam splitter. Bat-ear polarization controllers in the fibers ensure that the polarizations in both inputs are kept equal.

The two outputs of the fiber beam splitter are sent to Transition Edge Sensors (TES), which are calorimeters measuring photon energy and provide true photon-number resolution when detecting monochromatic light. They also provide near-unity intrinsic detection efficiency and zero intrinsic dark counts, making them ideally suited for low-light experiments. The TES output yields a time and number resolved detection record [30].

Our setup constitutes an interferometer measuring optical coherence between $\mathbf{r}_1$ and $\mathbf{r}_2$. Stable interferometry requires that mechanical fluctuations in the position of the optical fibers be kept within $\lambda/5 \approx 40$ nm. To achieve this, we isolate the optical fibers and optical flat within an acrylic box, with a small hole towards the laser diode to let light into the interferometer. The entire experiment is then isolated further in another box on a floating optical table.

Before comparing the precision of the Count scheme to the Traditional and Click schemes we discuss the accuracy of our estimates of $|\gamma|$ and $\phi$. We determine this via two methods: (i) we compare the MLE values of $|\gamma|$ and $\phi$ to the values calculated directly from the fringes; (ii) we use the MLE for $|\gamma|$ and the van Cittert–Zernike theorem to estimate the diameter of the source, and compare it to a directly measured value of the source diameter. We calculated $|\gamma| = 0.096$ using Eq. (1) and we found

TABLE I. Complex degree-of-coherence magnitude, $|\gamma|$, and phase, $\phi$, for the Count, Traditional, and Click schemes. The size of the spot is $a$, the distance between $\mathbf{r}_1$ and $\mathbf{r}_2$ is $d$, the wave number is $k$, the distance from the source to the collection points is $D$, and the angle to the centre of the spot is $\theta$ (see Supplemental Material [28]). Values are the average for datasets of sizes 1000 to 10 000.

| Scheme | $\lvert\gamma\rvert = \lvert \sin c(kda/2D)\rvert$ | $\phi = kd\theta$ |
|---|---|---|
| *Count* | $0.096 \pm 0.022$ | $4.32 \pm 0.25$ |
| *Click* | $0.095 \pm 0.025$ | $4.29 \pm 0.35$ |
| *Traditional* | $0.20 \pm 0.16$ | $4.5 \pm 1.0$ |

$\phi = 4.11$ rad from averaging the applied phase, $\phi_a$, at the extremal points for all fringes in the photon-number coincidence basis. For method (i), the visibility $|\gamma|$ was calculated from the average of only the [0,1] and [1,0] fringes. The higher order fringes were not included due to the presence of increased noise. Outliers in the data would inflate their visibility. The MLE does not suffer from this drawback. The method (i) calculated values for both $|\gamma|$ and $\phi$ are consistent with the results of the MLEs for all three schemes.

For method (ii) we measured the source diameter, which is equal to the spot size of the beam incident on the ground glass plate, see Fig. 2. The ground-glass plate was placed within $\pm 0.25$ mm of the beam waist. (The uncertainty in position is due to a small amount of precession of the rotating plate). Using a beam profiler we measured the spot size at the waist to be $15.3 \pm 0.1$ $\mu$m and the spot size 0.25 mm from the waist to be $18.0 \pm 0.1$ $\mu$m. We therefore expect to estimate a source diameter in the range 15.3–18.0 $\mu$m. Using the van Cittert–Zernike theorem and our estimated visibility we estimate the source diameter to be $16.5 \pm 0.5$ $\mu$m, agreeing well with the predicted range of diameters (see the Supplemental Material [28] for details).

Table I summarizes our estimates of the complex degree-of-coherence magnitude, $|\gamma|$, and phase, $\phi$, using the Count, Traditional, and Click schemes, averaged over dataset sizes from 100 to 10 000 points. For $|\gamma|$, the Count scheme is, respectively, 7.3 and 1.1 times more precise than the Traditional and Click schemes; for $\phi$, the Count scheme is, respectively, 4.0 and 1.4 times more precise than the Traditional and Click schemes. Moving beyond these averages, for the 10 000 point dataset, the Count scheme is over an order-of-magnitude more precise for $|\gamma|$, and four times more precise for $\phi$, than the Traditional scheme. These results also apply to comparisons between the Click and Traditional schemes since Fig. 3 displays that the Count and Click schemes are of approximately equivalent precision for larger dataset sizes. These results demonstrate that the Count and Click schemes are significantly better than the Traditional scheme, corroborating the result by Pearce *et al.* that the Count scheme is near-optimal among noncollective measurements [26]. Estimates for $|\gamma|$ and $\phi$ based on various data set sizes are shown in Figs. 3 and 4. They reveal that the Count scheme converges more quickly around the true values of $|\gamma|$ and $\phi$ than the Traditional scheme.

In the Traditional scheme we see a consistent bias in the $|\gamma|$ value estimates, relative to the Count or Click scheme. This is due to the uncertainty in $|\gamma|$ for the Traditional scheme being greater than the difference between the true $|\gamma|$, 0.096, and the lower limit of $|\gamma|$, zero. This results in the truncation of some MLE estimates smaller than $|\gamma|$, causing inflation of the mean $|\gamma|$ estimation.

Practical application of the Count scheme to the imaging of objects with arbitrary spatial configurations will require a two-dimensional array of photon-number-resolving detectors and phase varying elements. This setup could be realized by pairing a recent implementation of an array of photon-number-resolving detectors [31] along with a liquid crystal spatial light modulator to dynamically vary the phase of the light entering each detector. A reconstructed image is then formed by measuring the CDC between all detector pairs in the array and calculating the source distribution via the van Cittert–Zernike theorem. To demonstrate this method we simulated imaging of a complex object with a $26 \times 26$ array of detectors using the Count and Traditional methods (see Fig. 5). The simulation shows that the Count scheme results in images with improved contrast and clarity over traditional imaging methods. Results from the Click scheme (see Fig. 3) shows that, for large data sets, substituting the array of photon-number-resolving detectors for an array of

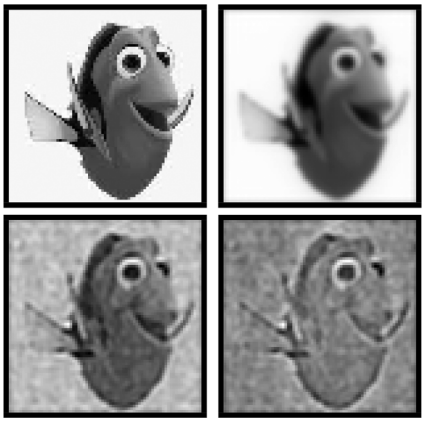

FIG. 5. Simulated comparison of images reconstructed using the Count and Traditional schemes for a $26 \times 26$ array of detectors. The Click scheme is not shown due to it, visually, looking very similar to the Count scheme. Top left: the original image before reconstructive imaging. Top right: reconstructed image in a noiseless regime, revealing the theoretical limits of the method. Bottom left: reconstructed image based on our Count scheme. Bottom right: reconstructed image based on the Traditional scheme. A detailed description of the simulation is given in the Supplemental Material [28].

non-photon-number-resolving detectors does not result in a large decrease in precision, and therefore may be a more economical alternative.

The Count and Click schemes, in contrast to intensity methods such as Hanbury Brown–Twiss interferometry, allows for estimation of both $|\gamma|$ and $\phi$, and hence total reconstruction of the source image (see Fig. 5). This, combined with their optimality in precision, their relative simplicity, and the ubiquity of interferometers in modern sensing and imaging technology, means that the Count and Click schemes have many potential applications. For example in astronomy these schemes open avenues to improved imaging of stellar bodies, with the Count scheme having a particular advantage due to its precision at low dataset sizes. Extension of the scheme to multiport interferometry [32] and the associated phase super-resolution may make possible imaging of previously inaccessible smaller bodies such as exoplanets, moons, and asteroids. In biology and medical imaging—through incorporation into interferometric reflectance schemes that detect reflected thermal light shone onto the source [33]—the Count and Click schemes can provide optimal imaging of small biological entities.

The authors would like to acknowledge helpful discussions from Marcelo Almeida. This work has been supported by the Australian Research Council (ARC) Center of Excellence for Engineered Quantum Systems (EQUS, CE170100009); the Engineering and Physical Sciences Research Council (EPSRC) via Grant No. EP/N014995/1 and the Quantum Communications Hub (Grant No. EP/M013472/1); and the University of Queensland by a Vice-Chancellor's Senior Research and Teaching Fellowship for AGW.

[1] V. Giovannetti, S. Lloyd, and L. Maccone, Advances in quantum metrology, Nat. Photonics **5**, 222 (2011).
[2] S. Ragy, M. Jarzyna, and R. Demkowicz-Dobrzański, Compatibility in multiparameter quantum metrology, Phys. Rev. A **94**, 052108 (2016).
[3] M. J. Rust, M. Bates, and X. Zhuang, Sub-diffraction-limit imaging by stochastic optical reconstruction microscopy (storm), Nat. Methods **3**, 793 (2006).
[4] E. Betzig, G. H. Patterson, R. Sougrat, O. W. Lindwasser, S. Olenych, J. S. Bonifacino, M. W. Davidson, J. Lippincott-Schwartz, and H. F. Hess, Imaging intracellular fluorescent proteins at nanometer resolution, Science **313**, 1642 (2006).
[5] M. Fernández-Suárez and A. Y. Ting, Fluorescent probes for super-resolution imaging in living cells, Nat. Rev. Mol. Cell Biol. **9**, 929 (2008).
[6] A. N. Boto, P. Kok, D. S. Abrams, S. L. Braunstein, C. P. Williams, and J. P. Dowling, Quantum Interferometric Optical Lithography: Exploiting Entanglement to Beat the Diffraction Limit, Phys. Rev. Lett. **85**, 2733 (2000).
[7] M. D'Angelo, M. V. Chekhova, and Y. Shih, Two-Photon Diffraction and Quantum Lithography, Phys. Rev. Lett. **87**, 777 (2001).
[8] Y. Shih, Quantum imaging, IEEE J. Sel. Top. Quantum Electron. **13**, 1016 (2007).
[9] S. Lloyd, Enhanced sensitivity of photodetection via quantum illumination, Science **321**, 1463 (2008).
[10] G. B. Lemos, V. Borish, G. D. Cole, S. Ramelow, R. Lapkiewicz, and A. Zeilinger, Quantum imaging with undetected photons, Nature (London) **512**, 409 (2014).
[11] S. Slussarenko, M. M. Weston, H. M. Chrzanowski, L. K. Shalm, V. B. Verma, S. W. Nam, and G. J. Pryde, Unconditional violation of the shot-noise limit in photonic quantum metrology, Nat. Photonics **11**, 700 (2017).
[12] M. Tsang, R. Nair, and X.-M. Lu, Quantum Theory of Superresolution for Two Incoherent Optical Point Sources, Phys. Rev. X **6**, 031033 (2016).
[13] J. S. Sidhu and P. Kok, Quantum metrology of spatial deformation using arrays of classical and quantum light emitters, Phys. Rev. A **95**, 063829 (2017).
[14] M. Tsang, Subdiffraction incoherent optical imaging via spatial-mode demultiplexing, New J. Phys. **19**, 023054 (2017).
[15] Z. S. Tang, K. Durak, and A. Ling, Fault-tolerant and finite-error localization for point emitters within the diffraction limit, Opt. Express **24**, 22004 (2016).
[16] W. K. Tham, H. Ferretti, and A. M. Steinberg, Beating Rayleigh's Curse by Imaging Using Phase Information, Phys. Rev. Lett. **118**, 070801 (2017).
[17] M. Paúr, B. Stoklasa, Z. Hradil, L. L. Sánchez-Soto, and J. Řeháček, Achieving the ultimate optical resolution, Optica **3**, 1144 (2016).
[18] F. Yang, A. Tashchilina, E. S. Moiseev, C. Simon, and A. I. Lvovsky, Far-field linear optical superresolution via heterodyne detection in a higher-order local oscillator mode, Optica **3**, 1148 (2016).
[19] J. Řehaček, Z. Hradil, B. Stoklasa, M. Paúr, J. Grover, A. Krzic, and L. L. Sánchez-Soto, Multiparameter quantum metrology of incoherent point sources: Towards realistic superresolution, Phys. Rev. A **96**, 062107 (2017).
[20] R. H. Brown and R. Q. Twiss, Correlation between photons in two coherent beams of light, Nature (London) **177**, 27 (1956).
[21] R. Schneider *et al.*, Quantum imaging with incoherently scattered light from a free-electron laser, Nat. Phys. **14**, 126 (2018).
[22] S. Oppel, T. Büttner, P. Kok, and J. von Zanthier, Superresolving Multiphoton Interferences with Independent Light Sources, Phys. Rev. Lett. **109**, 233603 (2012).
[23] M. E. Pearce, T. Mehringer, J. von Zanthier, and P. Kok, Precision estimation of source dimensions from higher-order intensity correlations, Phys. Rev. A **92**, 043831 (2015).
[24] M. Genovese, Real applications of quantum imaging, J. Opt. **18**, 073002 (2016).
[25] L. Mandel and E. Wolf, *Optical Coherence and Quantum Optics* (Cambridge University Press, Cambridge, England, 1995).
[26] M. E. Pearce, E. T. Campbell, and P. Kok, Optimal quantum metrology of distant black bodies, Quantum **1**, 21 (2017).

[27] C. W. Helstrom, Cramer-Rao inequalities for operator-valued measures in quantum mechanics, Int. J. Theor. Phys. **8**, 361 (1973).

[28] See the Supplemental Material at http://link.aps.org/supplemental/10.1103/PhysRevLett.123.143604 for details on phase characterisation, data analysis, source size and angle estimation, the maximum likelihood estimator, and imaging simulation.

[29] W. Martienssen and E. Spiller, Coherence and fluctuations in light beams, Am. J. Phys. **32**, 919 (1964).

[30] G. G. Gillett, A hardware signal processor for transition edge sensors, Ph.D. thesis, The University of Queensland, 2017.

[31] J. Ma, S. Masoodian, D. A. Starkey, and E. R. Fossum, Photon-number-resolving megapixel image sensor at room temperature without avalanche gain, Optica **4**, 1474 (2017).

[32] K. J. Resch, K. L. Pregnell, R. Prevedel, A. Gilchrist, G. J. Pryde, J. L. O'Brien, and A. G. White, Time-Reversal and Super-Resolving Phase Measurements, Phys. Rev. Lett. **98**, 223601 (2007).

[33] D. Sevenler, O. Avci, and M. S. Ünlü, Quantitative interferometric reflectance imaging for the detection and measurement of biological nanoparticles, Biomed. Opt. Express **8**, 2976 (2017).